Time-resolved dosimetry for validation of 4D dose calculation in PBS proton therapy

Kostiukhina, Natalia; Palmans, Hugo; Stock, Markus; Knopf, Antje-Christin; Georg, Dietmar; Knaeusl, Barbara

Published in:
Physics in Medicine and Biology

DOI:
10.1088/1361-6560/ab8d79

Publication date:
2020

Physics in Medicine & Biology

Time-resolved dosimetry for validation of 4D dose calculation in PBS proton therapy

To cite this article before publication: Natalia Kostiukhina *et al* 2020 *Phys. Med. Biol.* in press https://doi.org/10.1088/1361-6560/ab8d79

Time-resolved dosimetry for validation of 4D dose calculation in PBS proton therapy

N Kostiukhina[1,2], H Palmans[3,4], M Stock[3], A Knopf[5], D Georg[1,2], B Knäusl[1,2]

[1]Division Medical Radiation Physics, Department of Radiation Oncology, Medical University of Vienna / AKH Vienna, Vienna, Austria

[2]Christian Doppler Laboratory for Medical Radiation Research for Radiation Oncology, Medical University of Vienna, Vienna, Austria

[3]EBG MedAustron GmbH, Medical Physics, Wiener Neustadt, Austria

[4]National Physical Laboratory, Medical Radiation Science, Teddington, United Kingdom

[5]Department of Radiation Oncology, University Medical Center Groningen, University of Groningen, the Netherlands

E-mail: natalia.kostiukhina@meduniwien.ac.at

Abstract

4D dose calculation (4D-DC) is crucial for predicting the dosimetric outcome in the presence of intra-fractional organ motion. Time-resolved dosimetry can provide significant insights in 4D pencil beam scanning (PBS) dose accumulation and is therefore irreplaceable for benchmarking 4D-DC.

In this study a novel approach of time-resolved dosimetry using five pinpoint ionization chambers (IC) embedded in an anthropomorphic dynamic phantom was employed and validated against beam delivery details. Beam intensity variations as well as beam delivery time-structure were well reflected with an accuracy comparable to the temporal resolution of the IC measurements.

The 4D dosimetry approach was further applied for benchmarking 4D-DC implemented in the RayStation 6.99 treatment planning system. The agreement between computed values and measurements was investigated for: (i) partial doses based on individual breathing phases, and (ii) temporally distributed cumulative doses. For varied beam delivery and patient-related parameters the average unsigned dose difference for (i) was 0.04±0.03 Gy over all considered IC measurement values, while the prescribed physical dose was 2 Gy. By performing (ii), a strong effect of the dose gradient on measurement accuracy was observed. The gradient originated from scanned beam energy modulation and target motion transversal to the beam. Excluding measurements in the high gradient the relative dose difference between measurements and 4D dose calculations for a given treatment plan at the end of delivery was 3.5% on average and 6.6% at maximum over measurement points inside the target.

Overall, the agreement between 4D dose measurements in the moving phantom and retrospective 4D-DC was found to be comparable to the static dose differences for all delivery scenarios. The presented 4D-DC has been proven to be suitable for simulating treatment deliveries with various beam- as well as patient-specific parameters and can therefore be employed for dosimetric validation of different motion mitigation techniques.

1 Introduction

While pencil beam scanning (PBS) has the advantage of providing high target dose conformity, one of its downsides is that it complicates accurate treatment of intra-fractionally moving targets. Dynamic scanned beam delivery in the presence of target motion on a similar time scale can potentially cause the so-called interplay effect resulting in under- and over-dosage in the target region and/or unwanted irradiation of nearby organs at risk. In addition, tissue density variations in the beam path due to organ motion can affect the beam ranges and, therefore, dose distribution especially for lung cancer treatments. Motion mitigation techniques that have been developed to deal with these effects, such as gating, rescanning or treatment planning on internal target volumes (Bert and Durante, 2011), need to be extensively tested before being clinically implemented in proton therapy (Trnkova *et al.*, 2018).

Employing four-dimensional (4D) dose calculation (4D-DC) is crucial for predicting the dosimetric outcome for moving targets. Via 4D-DC, treatments can be simulated and analyzed with respect to the patient-specific motion characteristics as well as with respect to various beam delivery parameters. Generally, 4D-DC is based on organ motion data represented by 4D computed tomography (4D-CT) images. Knowing the treatment delivery sequence, dose contributions of single spots can be correlated with corresponding motion phases, resulting in sub-doses on each individual CT phase. Using deformable image registration, these doses can then be warped to a reference CT phase. Summing up all phase contributions a final 4D accumulated dose distribution can be obtained. Such an approach was used in several studies (Bert and Rietzel, 2007; Dowdell *et al.*, 2013; Engwall *et al.*, 2018; Meijers *et al.*, 2019) and recently became available in clinically used treatment planning systems (TPS). In the more advanced 4D dose calculation algorithm developed at the Paul Scherrer Institute (PSI, Switzerland) a dose grid is continuously deformed by using deforming vectors from 4D images like 4D-CT or 4D magnetic resonance imaging (4D-MRI) (Boye *et al.*, 2013; Zhang *et al.*, 2019).

Despite a number of 4D-DC simulation-based studies, the literature on experimental validations of 4D-DC is rather limited. Final 4D accumulated PBS doses were characterized by means of films (Bert *et al.*, 2008; Ciocca *et al.*, 2016; Meijers *et al.*, 2019), two-dimensional (2D) ionization chamber (IC) arrays (Pfeiler *et al.*, 2018; Hara *et al.*, 2017), three-dimensional (3D) IC array in a water phantom (Richter *et al.*, 2013) and a scintillating-CCD system (Krieger *et al.*, 2018). A noteworthy example of 4D dose verification in conventional radiotherapy was demonstrated by Gholampourkashi *et al.* (2017), where dose was measured by the RADPOS 4D dosimetry system (Cherpak *et al.*, 2009) consisting of a MOSFET dosimeter and an electromagnetic positioning sensor. In most cases the patient motion was realized by embedding detectors in a platform or another moving device, which allowed to simulate and measure the interplay effect. More realistic experimental setups with tissue substitutes in the beam path (Pfeiler *et al.*, 2018; Meijers *et al.*, 2019) enabled additional verification of the beam range calculation.

In the studies listed above, even though some detectors could perform time-resolved measurements, no temporal dosimetric analysis was considered. The use of a 2D IC array (Octavius SRS 1000, PTW-Freiburg, Germany) in time-separated mode was partially demonstrated by King *et al.* (2016) in his work on the validation of a gating technique for photon beam deliveries. Time-resolved dosimetry by a prototype 2D diode array (Sun Nuclear Corporation - Melbourne, FL USA) was applied for proton radiography in passive scattering proton beam (Testa *et al.*, 2013). By another 2D diode array (Delta4PT, Scandidos, Sweden) a dose reconstruction in time for VMAT treatment plans was tested (Ravkilde *et al.*, 2014). VMAT plan verification was also presented in Ehrbar *et al.* (2019) by means of three plastic scintillators for high time-resolution dose measurements in a liver phantom.

Following these examples from photon and passive scattering proton radiotherapy, 4D dosimetry can also provide significant insights in 4D PBS dose accumulation and can therefore be employed for extended

4D-DC validations. The aim of this work was to benchmark PBS proton beam 4D-DC against time-resolved dose measurements in a dynamic anatomy by simulating the interplay effect including soft and lung tissue in the beam path. An anthropomorphic breathing thorax phantom ARDOS (Advanced Radiation DOSimetry) (Kostiukhina *et al.*, 2017; Kostiukhina *et al.*, 2019) with five pinpoint ICs embedded inside and outside the target was employed. First, time-resolved dosimetry information (time stamps and dose per pulse) was verified against beam delivery details (*BD log-files*), followed by twofold comparison analysis of measured and simulated by 4D-DC dose values.

2 Materials and Methods

2.1 4D framework and measurement scenarios

2.1.1 Treatment facility and its infrastructure

The synchrotron-based pencil beam scanning system at the MedAustron Center for Ion Therapy and Research in Wiener Neustadt (Austria) was employed for the dosimetric measurements. It features a pulsed beam time structure with a maximal spill length of 5 s and spill interruption functionality. The particle fluence can be degraded to 10, 20, or 50% of the nominal beam transmission (further in the text denoted as degrader (deg.) 10, 20, and 50) in order to assure the applicability of a low number of particles per spot potentially required. Experiments were executed in a dedicated research irradiation room equipped with a patient couch controlled by the robotic arm (Exacure, BEC GmbH, Reutlingen, Germany), as well as a couch-mounted X-ray imaging system (ImagingRing™, medPhoton GmbH, Salzburg, Austria). Positioning and irradiation characteristics in this room are identical to the clinical irradiation rooms at MedAustron (Stock *et al.*, 2018). For the details of the phantom (re-)positioning, its accuracy and reproducibility, the reader is referred to Kostiukhina *et al.* (2019).

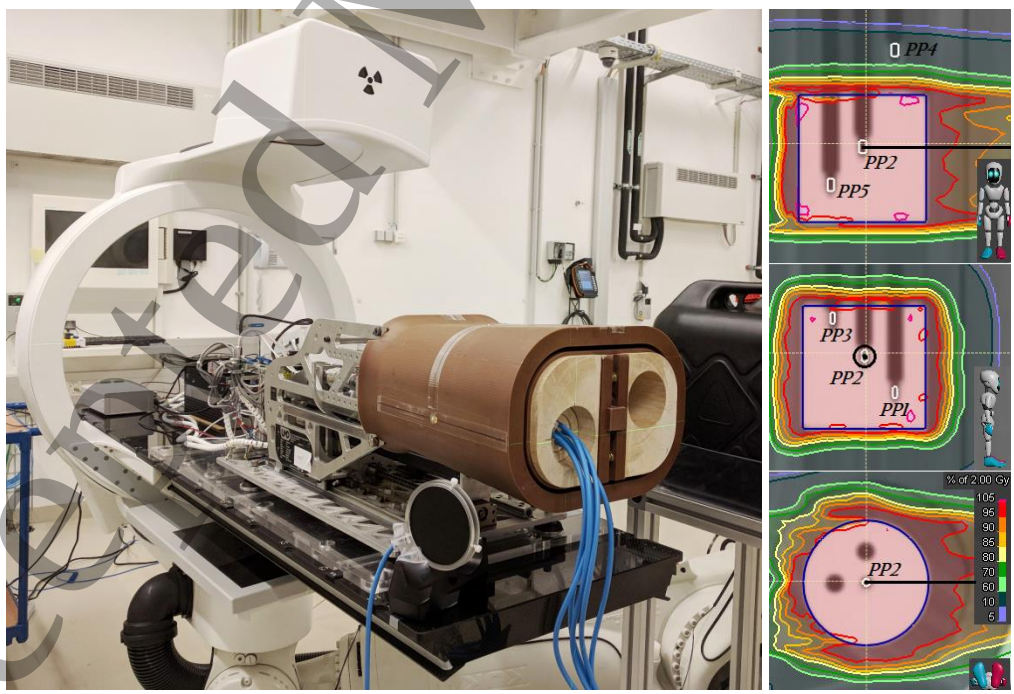

Figure 1 - (left) ARDOS phantom setup in the research irradiation room of MedAustron, positioned on the patient couch with integrated X-ray imaging system and including the positioning base plate; below the phantom the Bragg peak IC for measuring the time-check spots is visible; (right) CT images of the tumor replica (blue geometry) with five pinpoint IC positions marked (PP1-PP5) and iso-doses of the *primary* treatment plan with the beam direction shown in black

2.1.2 Phantom setup and CT imaging

The ARDOS phantom realistically represents the human thorax anatomy (Kostiukhina *et al.*, 2017) (figure 1). The phantom consists of the following tissue equivalent materials: solid water, cortical bone substitute, and balsa wood mimicking soft, rib, and lung tissue, respectively. The rigid materials and robust construction of the phantom enables submillimeter motion accuracy and reproducibility. The ARDOS feature of a moving rib cage was not used in this study to avoid additional influences on the dose distribution that are caused by the high density rib tissue interfaces. Digital linear position string encoders attached to each ARDOS motion axis, provide log-files (*ARDOS log-files*) that enable accurate determination of breathing and motion parameters. The ARDOS phantom was previously characterized extensively for dosimetry in proton beam therapy, including a validation of the tissue equivalence of the used materials, a determination of dose calculation accuracy in various lung set-ups and including a testing of detectors for proton dosimetry within the phantom (Kostiukhina *et al.*, 2019).

To keep the setup simple, only tumor motion in superior-inferior direction perpendicular to the beam was simulated in this study, while the other axes stayed static. Dose calculation for static and moving scenarios was based on CT images obtained by a Philips CT Brilliance Big Bore scanner (Philips Medical Systems, Andover, MA USA) and using the clinical acquisition protocol with a slice thickness of 0.1 cm. A CT scan of the static phantom with a tumor position corresponding to the exhale breathing phase was employed as a reference CT phase and was later on used for treatment planning. A 4D-CT of the phantom was composed of a stack of 3D images of the static ARDOS with 10 equidistant tumor positions simulating tumor motion over 10 phases covering the entire breathing cycle. Such approach of combining 3D images in order to obtain 4D-CT enabled to avoid image artifacts caused by motion, which can be crucial for 4D dose calculation.

2.1.3 Treatment planning for static phantom

In order to deliver a physical single-fraction dose of 2 Gy to the 97 cm^3 tumor volume, a *primary* single-beam treatment plan was created and further modified into various delivery scenarios. For that, the TPS RayStation 6.99 (RaySearch Laboratories AB, Stockholm, Sweden) with the Monte Carlo (MC) dose calculation algorithm version 4.1 was employed. The dose calculation accuracy was investigated by comparing the MC calculated doses against measurements performed in ARDOS material samples, which revealed less than 3% relative dose difference (Kostiukhina *et al.*, 2019). The superiority of the MC over analytical dose calculation algorithms for an anatomy with high tissue heterogeneities was demonstrated by dose differences of more than 20% calculated over the whole ARDOS geometry. In the current study, for all CT images the clinical CT calibration curve was applied and soft tissue represented by solid water was overwritten with known material parameters (atomic mass composition, mass density, and mean ionization energies). By this overriding procedure, the relative stopping power could be directly calculated, which increased the dose calculation accuracy as demonstrated by Kostiukhina *et al.* (2019). The clinical target volume (CTV) was defined as a cylinder with known dimensions of 5 cm height and 5 cm diameter corresponding to the size of the solid water tumor replica. Margins of 0.3 cm in superior-inferior direction and 0.5 cm in the other directions were used to define the planning target volume (PTV). The horizontally oriented proton beam crossed the phantom from the lateral direction before reaching the tumor. The degrader transmission for this *primary* treatment plan was set to 20% and a uniform voxel grid of $0.2\times0.2\times0.2$ cm^3 was used for the dose calculations. The *primary* treatment plan with the beam isocenter at the center of the PTV and a spot spacing of 0.3 cm, included 46 energy layers (67.5 - 115.0 MeV) and the number of protons per spot ranged from 0.9 to 47.5 $\cdot 10^6$.

2.1.4 Interplay (4D) dose calculation

4D dose calculation (4D-DC) was enabled via a scripting interface, integrated in the TPS through an incorporated IronPython console (Python Software Foundation, Wilmington, US). For retrospective 4D dose calculation of a treatment plan created on the static CT and delivered to the moving anatomy (i.e. interplay dose or 4D dose), detailed information about organ motion and beam delivery, as well as their correlation, was required. While organ motion was characterized by the 4D-CT images and the pre-defined breathing period of 5 s, beam delivery details were derived from the *BD log-files* with time resolution down to 5.0 μs. During irradiation the start of the phantom's motion was triggered by the beam-on signal from the accelerator enabling the definition of the breathing phase relative to the beam delivery start and thus assuring the repeatability of the experiment. By combining the information on organ motion, namely 4D-CT, start breathing phase and breathing period with the beam delivery details, each beam spot could be re-assigned to a certain breathing-phase CT and then partial doses could be calculated. For the next step of warping the partial doses to the reference CT phase and calculating the resulting dose distribution, deformable image registration (DIR) between each individual-phase CT and the reference-phase CT was employed. For that purpose the hybrid intensity and structure based DIR algorithm implemented in RayStation 6.99 was used.

2.1.5 Time-resolved dosimetry

The absorbed dose to water was determined inside and outside of the target volume using five pinpoint ionization chambers (PP) (type TM31015–0.03cm³–SN519-521,SN548-549, PTW-Freiburg, Germany), denoted PP1 to PP5, connected to a MULTIDOS multichannel electrometer (SN1583, PTW-Freiburg, Germany). Prior to the measurements the PPs were cross-calibrated against a reference Farmer chamber (type TM30013–0.6cm³–SN7258, PTW-Freiburg, Germany) connected to a UNIDOSwebline electrometer (SN883, PTW-Freiburg, Germany) in a 179.2 MeV proton beam at 2 cm depth in water, using a field size of 12×12 cm^2. To avoid partial shielding or scatter perturbation of the respective PPs within the ARDOS phantom, the volume of the tumor replica and distances between PPs were increased compared to our previous multi-PP measurement setup described in Kostiukhina *et al.* (2019). PP positions inside and outside of the tumor replica (figure 1) were verified prior and between dose deliveries by means of X-ray images obtained by the couch mounted X-ray system to make sure the chambers were not slipping out of the inserts during phantom motion.

Since recording dosimetric data in the time separated mode was not supported by the software of the MULTIDOS, communication via its RS-232 serial port was implemented to obtain time-resolved PP dose values. For that, a Python script was written in-house enabling recording ionization chamber readings in *dosimetry log-files* with 0.5 s time intervals. Each delivery scenario was measured 2-3 times.

In order to compare 4D-DC to the measurements, the calculated average doses in the respective regions of interest (ROI) corresponding to the detectors' positions and sensitive volumes (figure 1, right), were extracted. This method of ROI definition was applied throughout the study unless otherwise specified.

2.1.6 Measurement scenarios

For testing time-resolved dosimetry methods and validating 4D dose calculation approaches, beam delivery and patient-related parameters were varied and combined into different scenarios. The patient-related parameters included: target motion (static and periodic with 0.6 and 2.0 cm amplitude moving from the isocenter position cranially) and breathing phase relative to the beam delivery start (0, 25, and 75% of the breathing cycle). From the beam delivery parameters, the physical dose to the PTV (2 Gy as for a conventional fractionation scheme, and 4 Gy as for a hypofractionation scheme) and degradation of beam transmission (10, 20, and 50%) were varied.

2.2 Verification of 4D dosimetry approaches

Time-resolved dose measurements were evaluated in terms of synchronicity with the beam delivery (BD) time structure and the capability to reflect dosimetric changes due to beam intensity variations. The BD time structure comprised beam-on time intervals and beam pauses (figure 2, bottom). The spill interruption functionality enabled spill abortion after the prescribed amount of particles has been reached for a particular iso-energy layer. With this functionality the beam-on time depended directly on the treatment plan design (i.e. number and levels of energy layers, number of spots, and spot weights) and the chosen beam transmission degradation. In turn, the beam pauses were fixed to 5s.

2.2.1 Correlation with beam delivery time structure

An accurate alignment of the BD and the 4D dosimetry timelines could be achieved by time-check spots integrated into the treatment plans. These spots were located outside of the treatment field and could be measured with a Bragg Peak ionization chamber (PTW-Freiburg, Germany) positioned next to the ARDOS phantom (figure 1, left).

The spots were included into several energy layers over each treatment plan (layer number *1, 3, 12, 25, 32, 46*) and could be identified in the *dosimetry log-files* (combined for PPs and Bragg Peak IC) as well as the *BD log-files*. After delivery, time stamps of entries dedicated to each time-check spot were derived from both log-files and correlated to each other (figure 2).

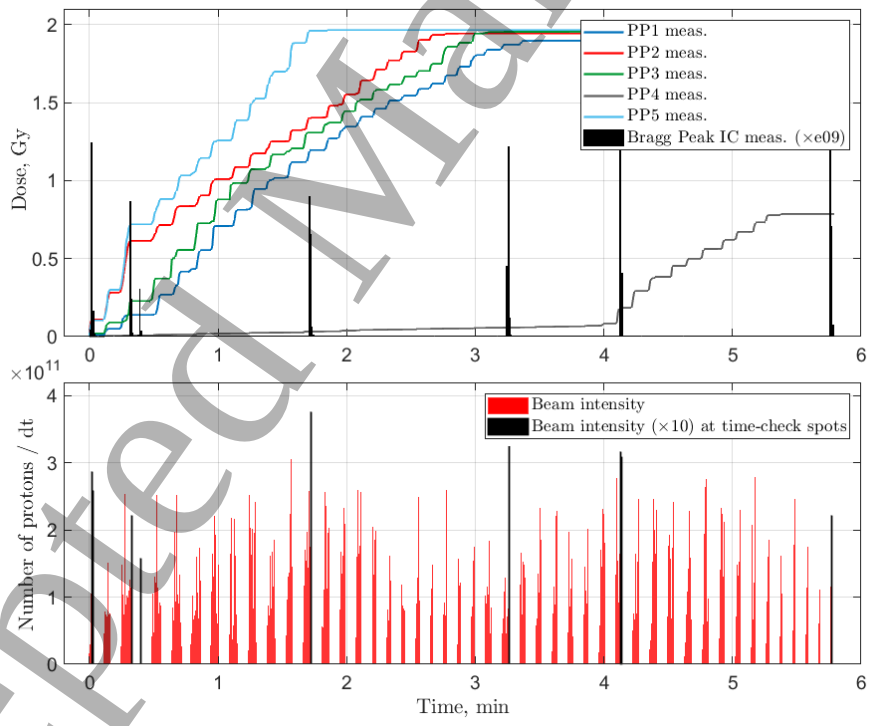

Figure 2 - (top) time-resolved measurement data from the *dosimetry log-files* and (bottom) beam intensities from the *beam delivery log-files*. Scenario - *primary* treatment plan (2 Gy, deg. 20) delivered to the static phantom. The figure demonstrates cross-correlation between timelines from the two types of log-files enabled by introducing time-check spots to treatment plans

2.2.2 Capability to reflect beam intensity variation

Time-averaged beam intensities I_i and their relative standard deviations RSD_i were evaluated for individual energy layers of each treatment plan as defined in equation (1) and (2). Additionally, the final accumulated

dose differences between deliveries of the same plan were calculated to explore the influence from the beam variation on the dose distribution.

$$I_i = Np_i / t_i, \quad (1)$$

$$RSD_i = \frac{SD(I_i,M)}{mean(I_i,M)} \cdot 100\%, \quad \text{for } i = 1 \dots E\,, \quad (2)$$

where Np_i is a measured number of protons per energy layer, t_i – irradiation time of the energy layer, both from *BD log-files*, E – number of energy layers, M – number of repeated measurements for a given scenario. In case of multiple spills required for an energy layer, beam-off time was excluded from the t_i.

2.3 Validation of 4D dose calculation

To validate computed dose values against measurements two dose interpreters were considered:

- partial doses for individual breathing phases (before accumulating them to the reference-phase CT), and
- temporally distributed cumulative doses in multiple points.

The more pronounced the interplay effect was, the more demonstrable comparison could be performed. Therefore, for the validation of 4D dose calculation only measurements with the target motion of 2.0 cm amplitude in combination with measurements in the static phantom as a reference were employed. Irradiation of the phantom with 0.6 cm target motion were not included into this evaluation as their dosimetric results did not significantly differ from the static deliveries (see *section 3.1*).

2.3.1 Partial doses for individual breathing phases

Calculation of partial doses for individual breathing phases was a required intermediate step in the 4D-DC algorithm. For being able to compare the calculated values with the measured ones, the latter had to be additionally post-processed. For doing so, the time-resolved measurement readout was split by the time interval equal to the breathing phase Δt_{ph} and the resulting dose fractions $D_{meas}\,(t_{ph})$ were distributed over bins of a number of breathing phases N_{ph}. Differences between computed and measured partial doses DD_{ph} were calculated according to equation (3) for all 17 deliveries to the moving target, 5 PPs and 10 breathing phases. The DD_{ph} were found to be sensitive to 0.1 - 0.5 s time offsets applied to the start time of the measurement, which are within the 0.5 s temporal resolution of IC measurements. Therefore, an offset giving the best match for each compared datasets was applied.

$$DD_{ph} = \left| D_{ph,meas} - D_{ph,calc} \right|, \quad (3)$$

$$D_{ph,meas} = \sum_{t_{ph}} D_{meas}\,(t_{ph}\,),$$

$$t_{ph} = \left[ph,\ ph + 1 \cdot N_{ph},\ ph + 2 \cdot N_{ph}, \dots \right], \quad \text{while } t_{ph} \le T, \quad \text{for } ph = 1 \dots N_{ph}\,,$$

where T is a total time of delivery.

2.3.2 Temporally distributed cumulative doses

In the second approach of 4D-DC validation, the 4D dose was derived for a number of time points ($t(E)$), homogeneously distributed over the treatment delivery. Each $t(E)$ was defined as the time of a complete delivery of a certain energy layer E and dose $D_{t(E),calc}$ was calculated for all energies delivered until $t(E)$ in descending order. In contrast to the previous method, the $D_{t(E),calc}$ was an accumulation of all partial doses transformed from each individual breathing-phase CT to the planning CT phase. To estimate the agreement between calculated and measured doses, the dose difference at $t(E)$ was introduced as follows:

$$DD_{t(E)} = \left|D_{t(E),meas} - D_{t(E),calc}\right|, \qquad \text{for } E = 2\text{ - }8, 10, 12, 15, 20, 25, 30, 35, 41. \tag{4}$$

As $t(E)$ for energy layer number E was dependent on the beam intensity, it was defined individually for each irradiation based on BD log-files. For calculating both DD_{ph} and $DD_{t(E)}$ for hypofractionated treatment deliveries, normalization to the conventional fractionation was used by applying a multiplication factor of ½.

Further, the dependency and possible reduction of $DD_{t(E)}$ were investigated by varying the used 4D-DC parameters such as size of dose calculation grid and region/point of interest (ROI/POI) for dose read-out. For that purpose, simulations of the *primary* treatment deliveries to static and moving phantom (2.0 cm target motion) were considered. ROI_1 (initial ROI) represented the inner cavity of a pinpoint IC in a form of a cylinder with a height of 0.50 cm and a radius of 0.15 cm (figure 1, right). Taking into account the air filling of the IC, the ROI_1 was modified to ROI_2 by reducing thickness of the region to 0.1 cm at the beam-entrance direction. POI was defined as a displacement of the PP central point on 0.75 times its inner radius (0.75R) to the side of beam incident as described in (Palmans, 2006; Sugama *et al.*, 2015). Among with initially applied dose calculation grid of 0.2×0.2×0.2 cm^3, a reduced one of 0.1×0.1×0.1 cm^3 was also considered.

Additionally, the dose gradient for each PP was determined in a sphere of 0.25 cm radius r with a center at the effective point of measurement following equation (5). The sphere size reflected the position shift of each measurement point due to the target motion amplitude of 2 cm. The gradient was defined on 3D (static) as well as 4D interplay dose distributions simulated for three deliveries of the *primary* treatment plan.

$$\frac{\Delta D_{x,y,z}}{2r} = \sqrt{\left(\frac{\Delta D_x}{2r}\right)^2 + \left(\frac{\Delta D_y}{2r}\right)^2 + \left(\frac{\Delta D_z}{2r}\right)^2} \tag{5}$$

3 Results

All measurement results are summarized in table 1. For measurements in the stationary phantom, the relative standard deviation of the final accumulated doses between iterations of all considered treatment plans was less than 0.7%.

3.1 Verification of 4D dosimetry approaches

3.1.1 Correlation with beam delivery time structure

The time stamps from *BD* and *dosimetry log-files* of the first time-check spot were synchronized. From that the time correlation for the other time-check spots was obtained and is presented in figure 3.

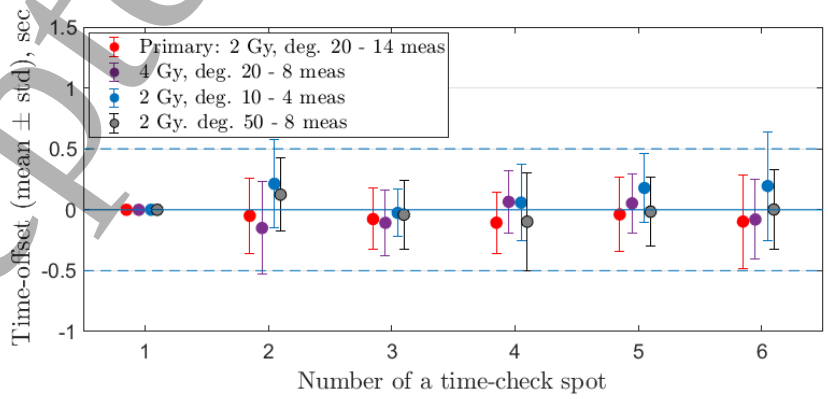

Figure 3 - offsets between time stamps from *beam delivery* and *dosimetry log-files*; shown for the six time-check spots and are grouped by the delivery type

3.1.2 Capability to reflect beam intensity variation

The RSD_i of beam intensities for respective energy layers between deliveries of the same treatment plan was 9% on average, and similar for all delivery types (table 1). The maximum variation was 56%, but only for a few energy layers per delivery. The total delivery time between repetitions of a given plan never varied more than 8%. The different pattern of spot distributions over breathing phases resulting from this beam intensity variation could be correlated to the dose differences at PP positions between deliveries of the same plans (figure 4). For the motion of 0.6 cm the dose difference was 1.8% at maximum for PP1-PP3 as well as PP5 located inside the target, but up to 5% for PP4 positioned outside of the target. The 2.0 cm motion amplitude could introduce dose differences of up to 30% depending on the PP position.

Table 1. Treatment plan specification, beam delivery parameters, beam intensity variation and results of dose measurements by five pinpoint ICs for various motion scenarios. All uncertainties are type A standard uncertainties; the overall uncertainty of the dose determination with the PP also combines 2.6% (Carlino *et al.*, 2018).

Treatment plan specification		Energy layers: 46 (67.5 - 115.0 MeV) Number of spots: 7735 Spot weight range*: 0.9-47.5 •10⁶ protons / spot			
Delivery type: prescribed physical single-fraction dose, beam transmission degradation		*Primary*: 2 Gy, deg. 20	4 Gy, deg. 20	2 Gy, deg. 10	2 Gy, deg. 50
Beam intensity variation (RSD_i), mean (min, max) [%]		9 (4, 44)	8 (2, 49)	7 (2, 39)	9 (5, 56)
Total treatment delivery time, mean ± SD [min]		5.79 ± 0.09	8.99 ± 0.22	14.02 ± 0.47	4.89 ± 0.05
Total dose for PP1-PP5, mean ± SD [Gy]	Phantom static	1.90 ± 0.00 1.94 ± 0.00 1.96 ± 0.00 0.78 ± 0.00 1.96 ± 0.00	3.78 ± 0.00 3.88 ± 0.00 3.90 ± 0.00 1.58 ± 0.00 3.91 ± 0.00	1.89 ± 0.01 1.95 ± 0.01 1.95 ± 0.01 0.81 ± 0.00 1.97 ± 0.01	1.90 ± 0.00 1.96 ± 0.00 1.96 ± 0.00 0.82 ± 0.00 1.97 ± 0.00
	Target motion - 0.6 cm amplitude	1.94 ± 0.02 1.98 ± 0.00 1.83 ± 0.01 0.48 ± 0.01 1.97 ± 0.02	3.85 ± 0.07 3.87 ± 0.05 3.76 ± 0.06 1.12 ± 0.05 3.91 ± 0.06	--	1.94 ± 0.01 1.94 ± 0.01 1.89 ± 0.01 0.61 ± 0.03 2.01 ± 0.02
	Target motion - 2.0 cm amplitude	1.89 ± 0.11** 1.91 ± 0.14** 1.06 ± 0.23** 0.26 ± 0.02** 1.96 ± 0.05**	3.70 ± 0.19 3.85 ± 0.04 2.03 ± 0.12 0.54 ± 0.07 3.79 ± 0.12	1.89 ± 0.09 1.78 ± 0.25 1.05 ± 0.31 0.28 ± 0.01 2.09 ± 0.11	1.90 ± 0.04 1.86 ± 0.04 1.12 ± 0.03 0.28 ± 0.07 1.93 ± 0.05

* - spot weight range is shown for 2 Gy prescribed physical single-fraction dose, the values will be doubled for 4 Gy prescribed dose
** - average value for scenarios with various breathing phase at the delivery start: 0, 25, 75% of the breathing cycle; otherwise only scenario with 0% start breathing phase was performed

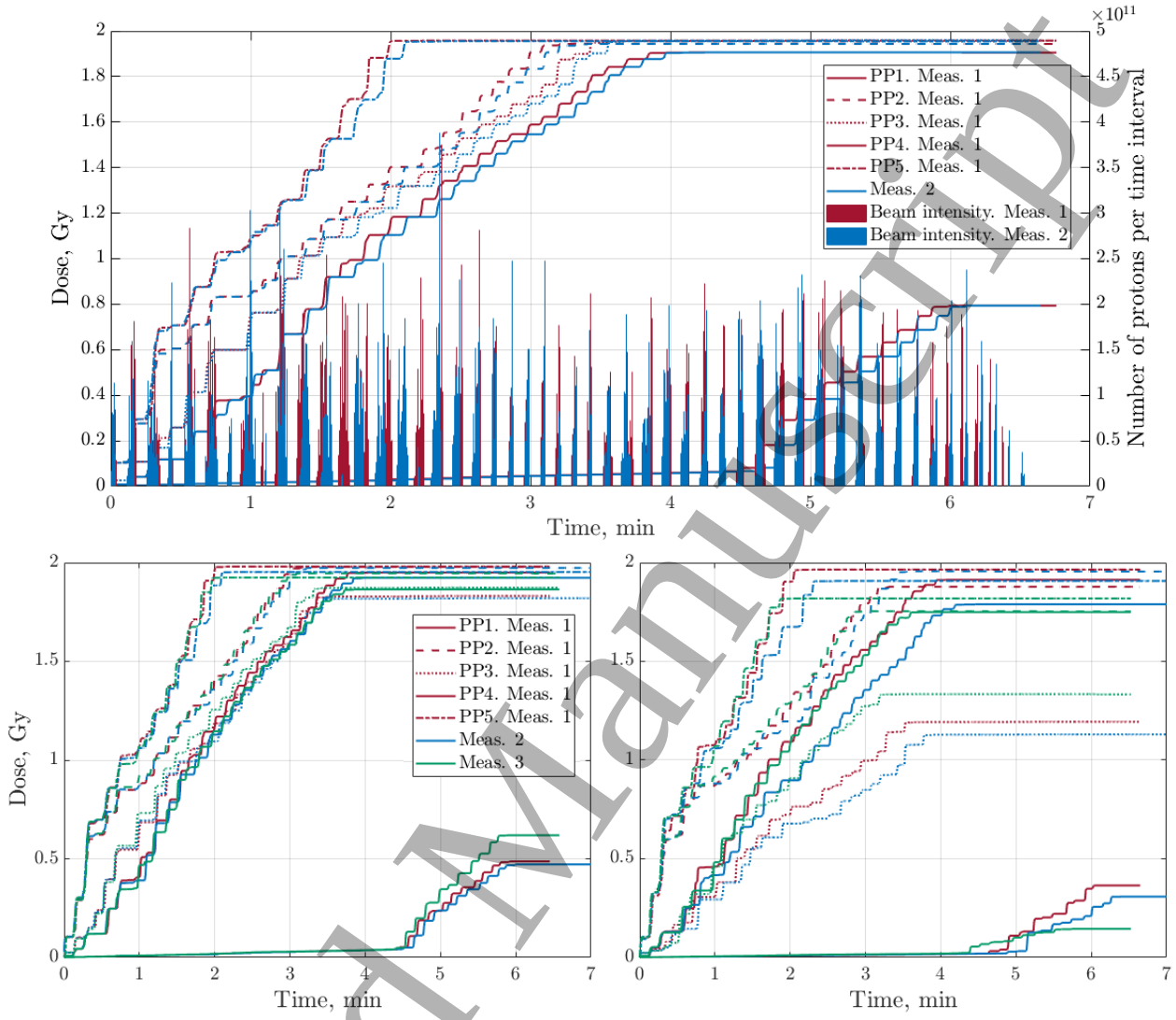

Figure 4 - (top) time-resolved dose measurements in the static phantom (2 measurements) by means of five PPs, correlated in time with beam intensities. (bottom) time-resolved dose measurements by means of five PPs in the presence of 0.6 cm (right) and 2.0 cm (left) target motion (3 measurements each). Scenario - *primary* treatment plan (2 Gy, deg. 20), breathing phase at the delivery start - 0% of the breathing cycle

3.2 Validation of 4D dose calculation

3.2.1 Partial doses for individual breathing phases

Figure 5 demonstrates examples of $D_{ph,calc}$ and $D_{ph,meas}$ for the *primary* and hypofractionated treatment deliveries along with their differences relative to the prescribed dose values. The average dose difference per phase DD_{ph} and its standard deviation over all measurements, PPs and phases were 0.04±0.03 Gy, which was 2% of the prescribed dose, and 20% of the prescribed-dose fraction (prescribed dose divided by the number of breathing phases). The DD_{ph} for different PPs did not vary significantly, except for PP4 as it measured outside the target: 0.04±0.03, 0.05±0.04, 0.04±0.04, 0.02±0.02, 0.04±0.03 Gy for PP1-PP5, respectively. Neither the beam delivery nor the patient related parameters had an influence on DD_{ph}. The dose distribution over the different phases was not uniform; however, most of the partial doses showed values lower than 0.4 Gy for the target PPs (PP1-PP3, and PP5) and 0.15 Gy for the outside-of-the-target PP4, for a fractionation of 2 Gy / fraction.

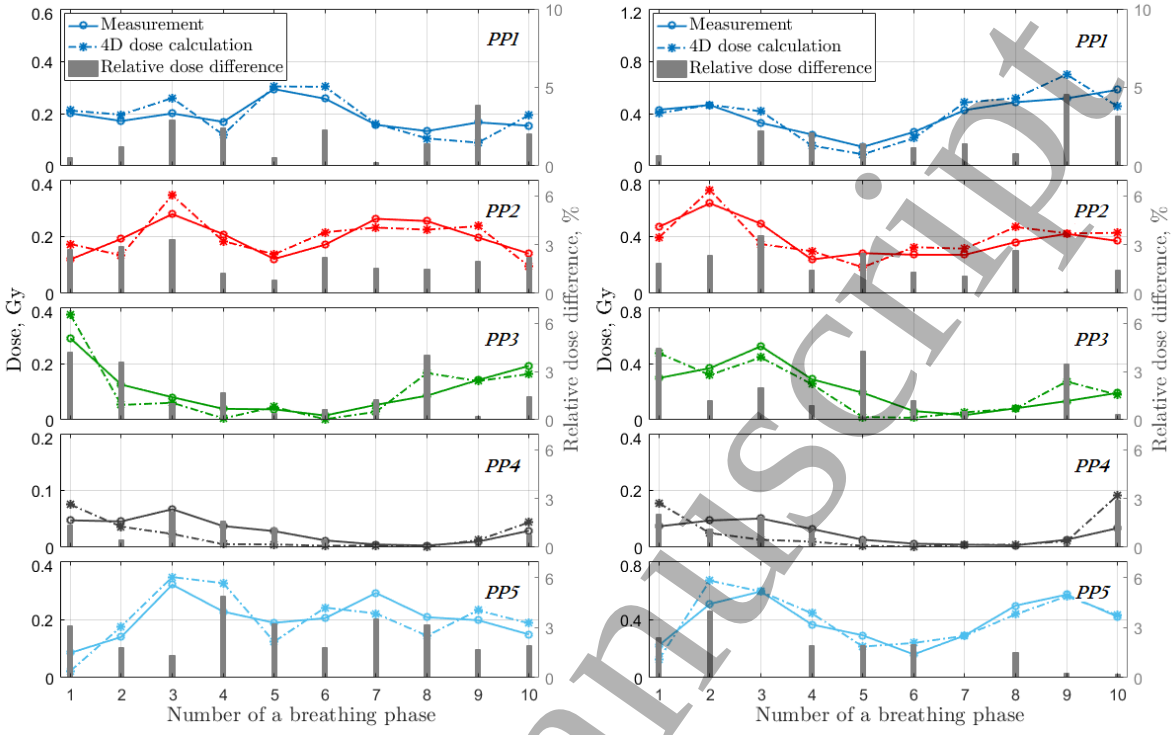

Figure 5 - 4D calculated partial doses for 10 individual breathing phases against measurements for (left) *primary* (2 Gy, deg.20) and (right) hypofractionated (4 Gy, deg.20) treatment deliveries. The respective dose differences are relative to the prescribed dose values. Colors represent the five PP measurement points. Lines are drawn to guide the eye

3.2.2 Temporally distributed cumulative doses

Figure 6 (left) gives $DD_{t(E)}$ for both static and moving cases, separately for each PP. For the measurement point outside of the target (PP4) the $DD_{t(E)}$ were below 0.06 Gy and 0.15 Gy over the full irradiation time for the static and moving deliveries, respectively. At the end of the plan delivery, the $DD_{t(E)}$ for the target PPs (PP1, PP2, PP3 and PP5) summed up to 0.08 Gy (4% of the 2 Gy prescribed dose) for static scenarios and to 0.30 Gy - for moving scenarios. These $DD_{t(E)}$ of static and moving cases increased over irradiation time until a certain moment, after which the $DD_{t(E)}$ stabilized at a plateau. Before the peaks of the $DD_{t(E)}$ distributions, the moving scenarios did not vary from the static ones for all target PPs. The plateau stabilized at higher values for PP2 and PP3.

Changing the read-out area from ROI_1 to ROI_2 did not influence $DD_{t(E)}$, while reading out the dose at the effective points of measurement reduced $DD_{t(E)}$ at maximum by 0.06 Gy (figure 7). Dose recalculated on 0.1×0.1×0.1 cm^3 grid reduced the $DD_{t(E)}$ on average by 1%.

Dose gradients for static and moving deliveries of the *primary* treatment plan are presented in figure 6 (right). A strong correlation between $DD_{t(E)}$ and corresponding dose gradients was observed. The highest gradient values of up to 1 Gy/cm were found for PP2 and PP3.

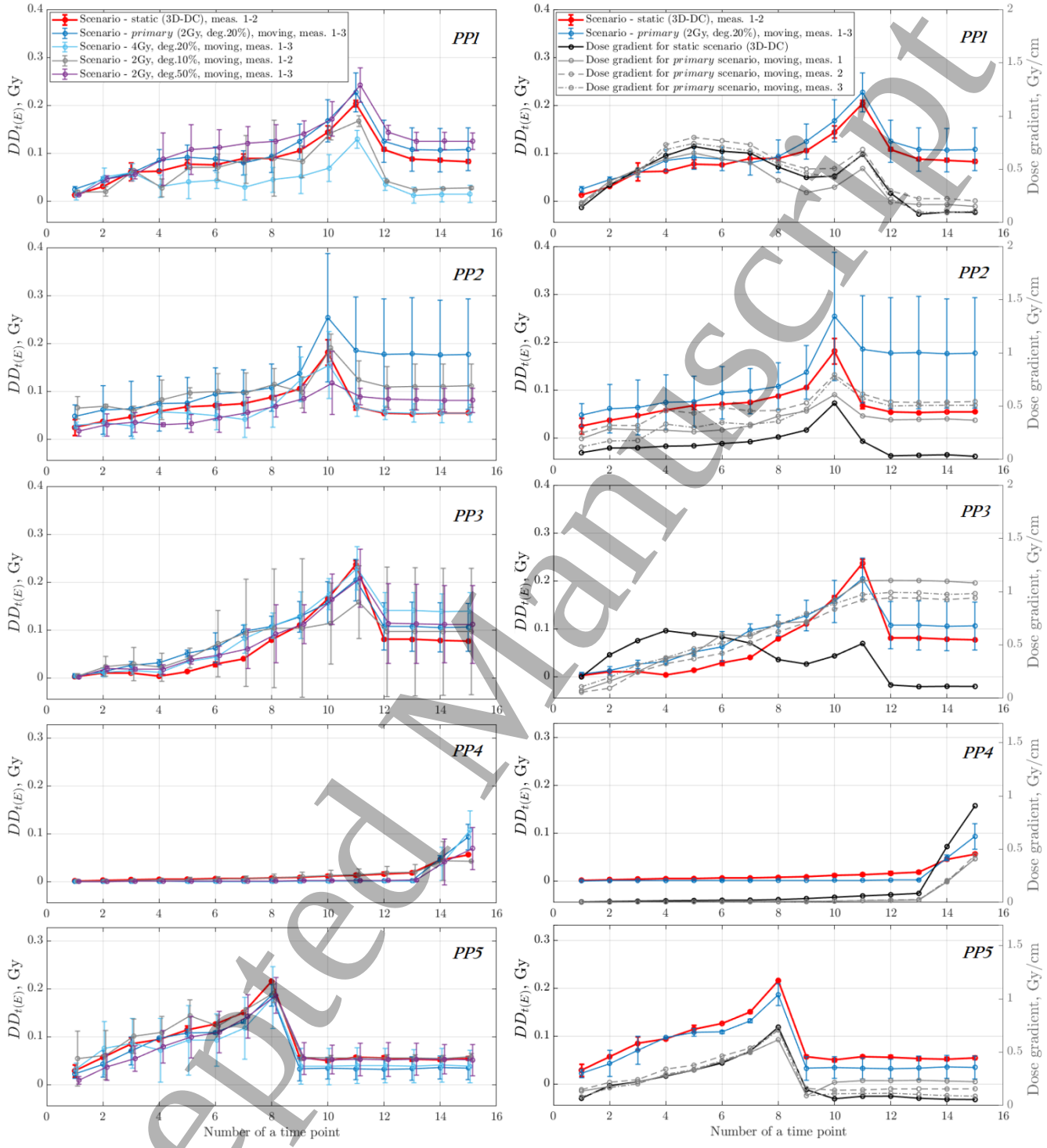

Figure 6 - (left) dose difference $DD_{t(E)}$ for static and moving scenarios and for all considered delivery types, shown for five PPs separately; (right) exemplary dose gradient for static and moving deliveries of the *primary* treatment plan (2 Gy, deg.20), presented separately for each measurement, shown along with the dose difference $DD_{t(E)}$ for the same scenarios

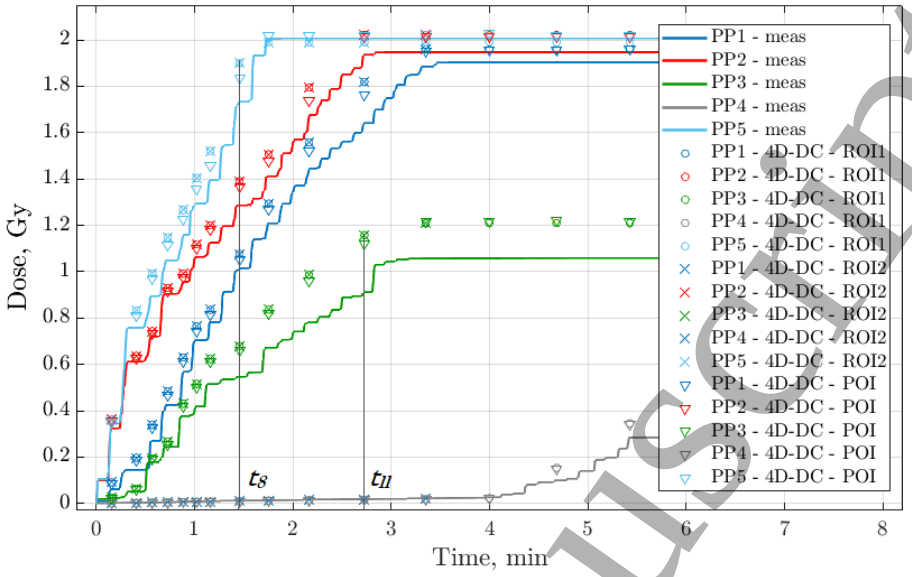

Figure 7 - exemplary results of time-resolved dose measurements by means of five PPs positioned inside (*PP1-3,5 - meas*) and outside (*PP4 - meas*) of the target; 4D dose calculation derived for 15 time points at ROI_1, ROI_2 and POI (*PP1-PP5 - 4D-DC - ROI1/ROI2/POI*). Scenario - *primary* treatment plan (2 Gy, deg.20) delivered to the moving (2 cm target motion) phantom, breathing phase at the delivery start - 0% of the breathing cycle

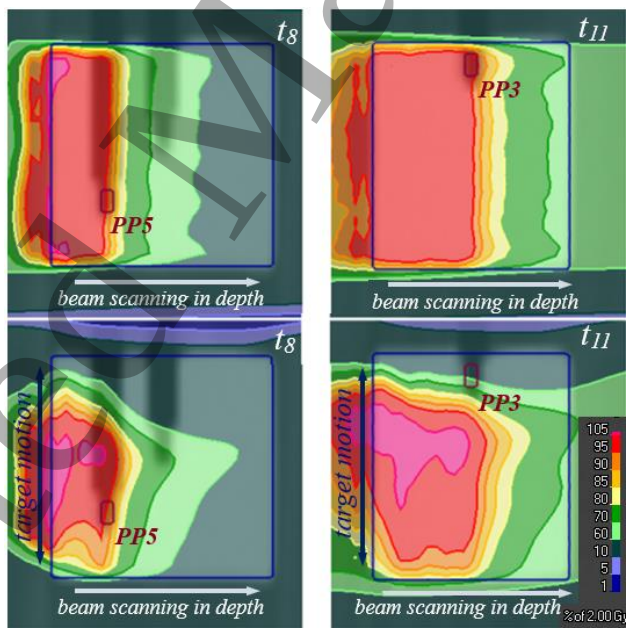

Figure 8 - dose distributions obtained by 4D-DC at the time points t_8 and t_{11}, for a *primary* treatment plan (2 Gy, deg.20) deliveried to the (top) static and (bottom) moving (2 cm target motion) phantom

4 Discussion

In this study a novel time-resolved dosimetry approach was introduced and benchmarked against temporally distributed beam delivery events. PP measurements in a static phantom were reproducible within 0.7% of the measured values. With 0.5 s temporal resolution of the PP measurements the time consistency between the incident spots and the resulting measurement events was essential. By registering the time stamps of dedicated time-check beam spots derived from *BD* and *dosimetry log-files*, the differences in the time

sequences were within ±0.5 s and no accumulation of differences were observed. Time-resolved PP measurements could reflect beam intensity variations by the respective consequences on the dose accumulation. For synchrotron based particle therapy, beam intensity variations can substantially influence the dose distribution in the presence of target motion and have to be taken into account when predicting the dose accumulation in time and when deciding on possible motion compensation techniques. For all considered delivery types the novel 4D dosimetry approach showed to be suitable for cutting-edge research projects aiming towards clinical end-to-end testing.

The PP based 4D dosimetry method was further applied for extensive validation of the 4D dose calculation algorithm implemented in the RayStation TPS by making use of its scripting interface. The first approach of the twofold analysis was focusing on sub-doses distributed to the individual breathing phases defined by a 4D-CT. This method was found to be sensitive to factors associated with post-processing of the measurement data, i.e. assigning the dose values to the dedicated breathing phases. Among them is an accurate definition of a breathing phase at the start of measurements. It is challenging due to similar order of the breathing phase length (~0.5 s) and temporal resolution of IC measurements (0.5 s). Another factor is the determination of the actual breathing period in relation to the measurements. Thanks to the *ARDOS log-files*, recorded periods could be applied for the retrospective calculation. However, in case of even small uncertainties in the breathing period definition, both the measured and calculated partial dose values would be affected and their relative differences could significantly increase. The importance of an accurate definition of the breathing period and starting phase was also emphasized by others (Pfeiler *et al.*, 2018), where sensitivity tests of cumulative doses at the end of delivery with respect to manipulated values of the considered parameters were performed. It is worth to note that in the present study the resulted partial dose values of the measurements deviated less from phase to phase than the ones calculated by 4D-DC, which makes the guiding lines look smoother (figure 5). This can be due to the limited temporal resolution of 4D-CT, which might compromise accuracy of 4D dose calculation as it was recently demonstrated in a comprehensive study of Zhang *et al.* (2019).

In the second approach temporal dose accumulations were computed by transferring to and summing up partial doses on the reference CT phase. These values were compared to the measurements at several time points during delivery resulting in cumulative $DD_{t(E)}$. The $DD_{t(E)}$ for static deliveries at the end of delivery were below 4% relative to the prescribed dose (figure 6). This could reflect measurement accuracy as well as TPS calculation tolerance for small targets in agreement with our previous study, where the phantom was commissioned for dosimetry in proton beams (Kostiukhina *et al.*, 2019). The peaks of static $DD_{t(E)}$ distributions in time were associated with certain proton energies and, therefore, with dose gradients in the beam direction (figure 8, top). When Bragg peaks occurred in a small proximity to the PP measurement points (for example, t_8 for PP5, t_{10} and t_{11} for PP1-PP3) even a small geometric deviation in the submillimeter range between real PP measurement positions and their simulations could introduce a noticeable difference between the dose values. Protons of the upcoming layers with lower energies further filled the target with dose making potential displacements negligible and hardly affecting $DD_{t(E)}$ at the end of delivery. The outside-of-the-target position of PP4 explains its different $DD_{t(E)}$ behavior compared to the other PPs. In the moving phantom steep dose gradients occurred also in the direction of target motion (figure 8, bottom), which additionally compromised measurement accuracy. In contrast to the gradient in beam direction of each individual energy layer, which will be compensated when the delivery of all layers is completed, the dose gradient due to target motion affected the $DD_{t(E)}$ until the end of delivery. Measurement points of PP2 and PP3 moving in-and-out of the high dose area were most affected by this interplay process, while PP1 and PP5 stayed either in or out of the irradiation volume. The lower beam transmission (deg.10) elongated the delivery time and, therefore, the number of motion cycles per delivery, which in turn enhanced the $DD_{t(E)}$ for PP2 and PP3.

By applying the 0.4 Gy/cm dose gradient threshold used for patient specific quality assurance at the MedAustron (Carlino *et al.*, 2019) in order to exclude measurements in the high gradient region, the relative dose difference (RDD) between measurements and 4D dose calculations for the *primary* treatment plan at the end of delivery was 3.5% on average and 6.6% at maximum over measurement points inside the target. In comparison, the RDD of 7.6% on average was reported by Pfeiler *et al.* (2018), where interplay dose was simulated and measured by 2D IC array. Richter *et al.* (2013) obtained 7% of RDD at maximum for gated deliveries measured with a 3D IC array. According to the interplay and rescanning study of Krieger *et al.* (2018), 5% of RDD was reached by 6.2% of analyzed area of the scintillating-CCD.

No significant difference was observed by changing the dose calculation grid from $0.2\times0.2\times0.2$ cm^3 to $0.1\times0.1\times0.1$ cm^3 as well as by changing ROI_1 to ROI_2. However, reading out dose at the effective point of measurements could improve the results and will be used for upcoming studies. Further advancements of the study will be including ribs to the moving anatomy as well as introducing complex irregular motion patterns of the torso and the tumor itself. Based on the established 4D-DC and time-resolved dosimetry the impact of different beam parameters as well as implementation of rescanning and gating motion compensation techniques will be investigated with the aim to reduce the impact of target motion and beam intensity variation.

5 Conclusion

The novel approach of time-resolved dosimetry was able to reflect beam delivery time-structure as well as intensity variations, and capable to validate 4D-DC in a synchrotron based proton therapy center.

The agreement between 4D dose measurements in the moving phantom and retrospective 4D-DC was found to be comparable to the static dose differences for all delivery scenarios. The exceptionally high dose differences for measurement points at the treatment field border could be explained by steep dose gradients in the beam direction and the ones originating from target motion transversal to the beam.

Similar results were observed between measured and 4D calculated doses in both, breathing-phase based as well as temporally-distributed cumulative, dose analyses when varying beam intensity degradation, fraction dose, and start of breathing relative to the start of beam delivery. Therefore, 4D-DC has been proven to be adequate for simulating treatment deliveries with various beam- as well as patient-specific parameters and can serve as a base for investigating motion compensation techniques.

Acknowledgments

The authors thank Simon E. Waid from EBG MedAustron and Andreas F. Resch from Medical University of Vienna for their support in implementing the functionality to obtain beam delivery and dosimetry log-files. The financial support by the (Austrian) Federal Ministry for Digital and Economic Affairs and the National Foundation for Research, Technology and Development is gratefully acknowledged.

References

Bert C and Durante M 2011 Motion in radiotherapy: particle therapy *Phys Med Biol* **56** R113-44

Bert C, Grozinger S O and Rietzel E 2008 Quantification of interplay effects of scanned particle beams and moving targets *Phys Med Biol* **53** 2253-65

Bert C and Rietzel E 2007 4D treatment planning for scanned ion beams *Radiat Oncol* **2** 24

Boye D, Lomax T and Knopf A 2013 Mapping motion from 4D-MRI to 3D-CT for use in 4D dose calculations: a technical feasibility study *Med Phys* **40** 061702

Carlino A, Bohlen T, Vatnitsky S, Grevillot L, Osorio J, Dreindl R, Palmans H, Stock M and Kragl G 2019 Commissioning of pencil beam and Monte Carlo dose engines for non-isocentric treatments in scanned proton beam therapy *Phys Med Biol* **64** 17nt01

Carlino A, Stock M, Zagler N, Marrale M, Osorio J, Vatnitsky S and Palmans H 2018 Characterization of PTW-31015 PinPoint ionization chambers in photon and proton beams *Phys Med Biol* **63** 185020

Cherpak A, Ding W, Hallil A and Cygler J E 2009 Evaluation of a novel 4D in vivo dosimetry system *Med Phys* **36** 1672-9

Ciocca M, Mirandola A, Molinelli S, Russo S, Mastella E, Vai A, Mairani A, Magro G, Pella A, Donetti M, Valvo F, Fossati P and Baroni G 2016 Commissioning of the 4-D treatment delivery system for organ motion management in synchrotron-based scanning ion beams *Phys Med* **32** 1667-71

Dowdell S, Grassberger C, Sharp G C and Paganetti H 2013 Interplay effects in proton scanning for lung: a 4D Monte Carlo study assessing the impact of tumor and beam delivery parameters *Phys Med Biol* **58** 4137-56

Ehrbar S, Johl A, Kuhni M, Meboldt M, Ozkan Elsen E, Tanner C, Goksel O, Klock S, Unkelbach J, Guckenberger M and Tanadini-Lang S 2019 ELPHA: Dynamically deformable liver phantom for real-time motion-adaptive radiotherapy treatments *Med Phys* **46** 839-50

Engwall E, Glimelius L and Hynning E 2018 Effectiveness of different rescanning techniques for scanned proton radiotherapy in lung cancer patients *Phys Med Biol* **63** 095006

Gholampourkashi S, Vujicic M, Belec J, Cygler J E and Heath E 2017 Experimental verification of 4D Monte Carlo simulations of dose delivery to a moving anatomy *Med Phys* **44** 299-310

Hara Y, Furukawa T, Tansho R, Saraya Y, Mizushima K, Saotome N, Shirai T and Noda K *Proceedings of the 4th International Beam Instrumentation Conference, IBIC 2015,2017),* vol. Series*)* pp 62-5

King R B, Agnew C E, O'Connell B F, Prise K M, Hounsell A R and McGarry C K 2016 Time-resolved dosimetric verification of respiratory-gated radiotherapy exposures using a high-resolution 2D ionisation chamber array *Phys Med Biol* **61** 5529-46

Kostiukhina N, Georg D, Rollet S, Kuess P, Sipaj A, Andrzejewski P, Furtado H, Rausch I, Lechner W, Steiner E, Kertesz H and Knausl B 2017 Advanced Radiation DOSimetry phantom (ARDOS): a versatile breathing phantom for 4D radiation therapy and medical imaging *Phys Med Biol* **62** 8136-53

Kostiukhina N, Palmans H, Stock M, Georg D and Knäusl B 2019 Dynamic lung phantom commissioning for 4D dose assessment in proton therapy *Phys Med Biol* **64** 235001

Krieger M, Klimpki G, Fattori G, Hrbacek J, Oxley D, Safai S, Weber D C, Lomax A J and Zhang Y 2018 Experimental validation of a deforming grid 4D dose calculation for PBS proton therapy *Phys Med Biol* **63** 055005

Meijers A, Jakobi A, Stutzer K, Guterres Marmitt G, Both S, Langendijk J A, Richter C and Knopf A 2019 Log file-based dose reconstruction and accumulation for 4D adaptive pencil beam scanned proton therapy in a clinical treatment planning system: Implementation and proof-of-concept *Med Phys* **46** 1140-9

Palmans H 2006 Perturbation factors for cylindrical ionization chambers in proton beams. Part I: corrections for gradients *Phys Med Biol* **51** 3483-501

Pfeiler T, Baumer C, Engwall E, Geismar D, Spaan B and Timmermann B 2018 Experimental validation of a 4D dose calculation routine for pencil beam scanning proton therapy *Z Med Phys* **28** 121-33

Ravkilde T, Keall P J, Grau C, Hoyer M and Poulsen P R 2014 Fast motion-including dose error reconstruction for VMAT with and without MLC tracking *Phys Med Biol* **59** 7279-96

Richter D, Schwarzkopf A, Trautmann J, Kramer M, Durante M, Jakel O and Bert C 2013 Upgrade and benchmarking of a 4D treatment planning system for scanned ion beam therapy *Med Phys* **40** 051722

Stock M, Georg D, Ableitinger A, Zechner A, Utz A, Mumot M, Kragl G, Hopfgartner J, Gora J, Bohlen T, Grevillot L, Kuess P, Steininger P, Deutschmann H and Vatnitsky S 2018 The technological basis for adaptive ion beam therapy at MedAustron: Status and outlook *Z Med Phys* **28** 196-210

Sugama Y, Nishio T and Onishi H 2015 Technical Note: Experimental determination of the effective point of measurement of two cylindrical ionization chambers in a clinical proton beam *Med Phys* **42** 3892-5

Testa M, Verburg J M, Rose M, Min C H, Tang S, Bentefour el H, Paganetti H and Lu H M 2013 Proton radiography and proton computed tomography based on time-resolved dose measurements *Phys Med Biol* **58** 8215-33

Trnkova P, Knausl B, Actis O, Bert C, Biegun A K, Boehlen T T, Furtado H, McClelland J, Mori S, Rinaldi I, Rucinski A and Knopf A C 2018 Clinical implementations of 4D pencil beam scanned particle therapy: Report on the 4D treatment planning workshop 2016 and 2017 *Phys Med* **54** 121-30

Zhang Y, Huth I, Weber D C and Lomax A J 2019 Dosimetric uncertainties as a result of temporal resolution in 4D dose calculations for PBS proton therapy *Phys Med Biol* **64** 125005